Supplementary Information

Molecularly imprinted polymer based electrochemical sensor for quantitative detection of SARS-CoV-2 spike protein

Akinrinade George Ayankojo, Roman Borozniak, Jekaterina Reut, Andres Öpik, Vitali Syritski

Department of Materials and Environmental Technology, Tallinn University of Technology, Ehitajate tee 5, 19086 Tallinn, Estonia.

*corresponding author e-mail: vitali.syritski@taltech.ee

S1. Covalent imprinting approach for ncovS1 recognition

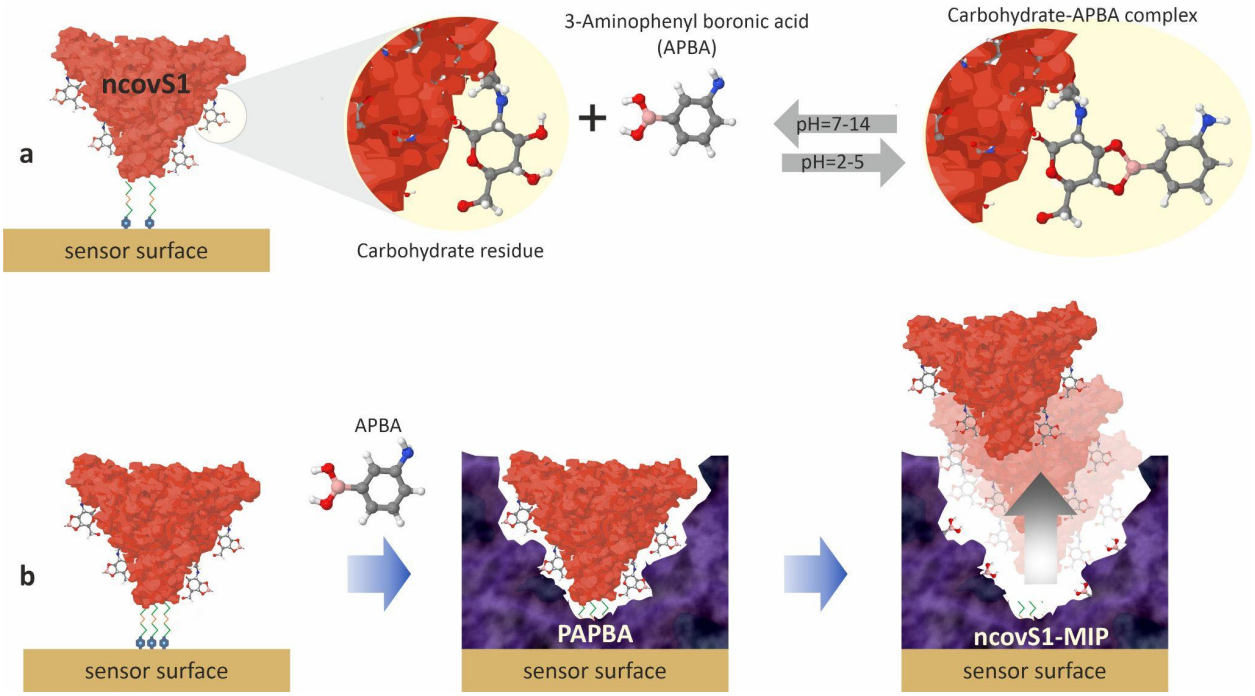

Fig. S1. a) Scheme showing the covalent interaction of the carbohydrate groups (red spheres) of glycosylated ncovS1 with the boronic acid group of 3-aminophenylboronic acid. b) Formation of ncovS1-MIP on the sensor surface by electropolymerization of APBA and subsequent removal of ncovS1 from the polymer (PAPBA).

S2. Characterization of sensor preparation

Electrochemical characterization

We monitored every stage of the sensor preparation by measuring both CV and SWV voltammograms to correlate each modification or treatment with the resulting changes in charge exchange between the redox pair and the Au-TFME surface. CV (Fig. S2(a)) shows a significant depression of the anodic and cathodic current peaks following DTSSP and ncovS1 immobilization on Au-TFME via ATP covalent attachment. Moreso, after electrodeposition of PAPBA, these peaks completely disappeared indicating the formation of a non-conducting polymer film on the electrode. Similar result is displayed by SWV (Fig. S2(b)) where the anodic current peak significantly decreases after DTSSP and ncovS1 immobilization with a complete disappearance following PAPBA electrodeposition.

To remove the entrapped ncovS1, the modified Au-TFME must undergo two consecutive treatments including 30 min in dithiothreitol (DTT) to break the disulfide bridge anchoring the ncovS1 to the Au-TFME, followed by 30 min treatment in acetic acid to remove the protein molecules. As observed, a re-emergence of the CV anodic and cathodic peaks (Fig. S2(a)), and SWV anodic peak (Fig. S2(b)) were seen after a combined treatments in DTT and acetic acids to form ncovS1-MIP. Although after ncovS1-MIP formation, lower levels of the peaks, in comparison to that following ncovS1 immobilization, were observed. This indicates that the increase in charge transfer recorded is due to the formation of microscopic ncovS1 permeable pathways within the polymer rather than the removal of the polymer film from Au-TFME. Thus, these results establish the successful formation of ncovS1-MIP film on Au-TFME that would be subsequently used as ncovS1 sensor.

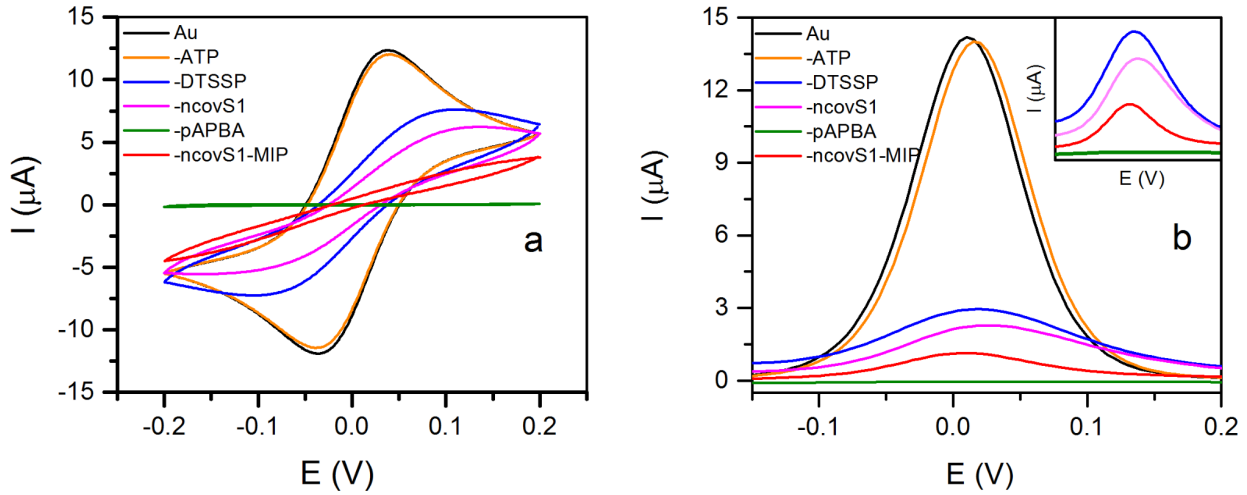

Fig. S2. Cyclic and square wave voltammograms recorded in 1 M KCl solution containing a 4 mM redox probe $K_3[Fe(CN)_6]/K_4[Fe(CN)_6]$ on bare Au (black), and after subsequent fabrication steps of ncovS1-MIP: modification by 4-ATP (orange), DTSSP (blue), and ncovS1 (magenta), electrodeposition of PAPBA (olive) and after treatment in DTT and acetic acid to form ncovS1-MIP (red).

Morphological characterization

Microscopic analysis was conducted using scanning electron microscopy (SEM) to observe the morphological changes occurring on the film following ncovS1-MIP formation. The SEM images of the bare, polymer modified electrode before template removal and ncovS1-MIP film modified electrodes are shown in Fig. S3. As observed, a morphological difference could be seen between the bare and polymer film modified electrodes however, there is an insignificant difference in the SEM images of PAPBA modified gold before (B) and after (C) treatments with acetic acid to form ncovS1-MIP. This is rather not surprising as we considered initially that the ncovS1-MIP film is too thin to allow for accurate scanning by microscopic techniques thereby preventing any meaningful differentiation in the morphological features of the film before and after treatments.

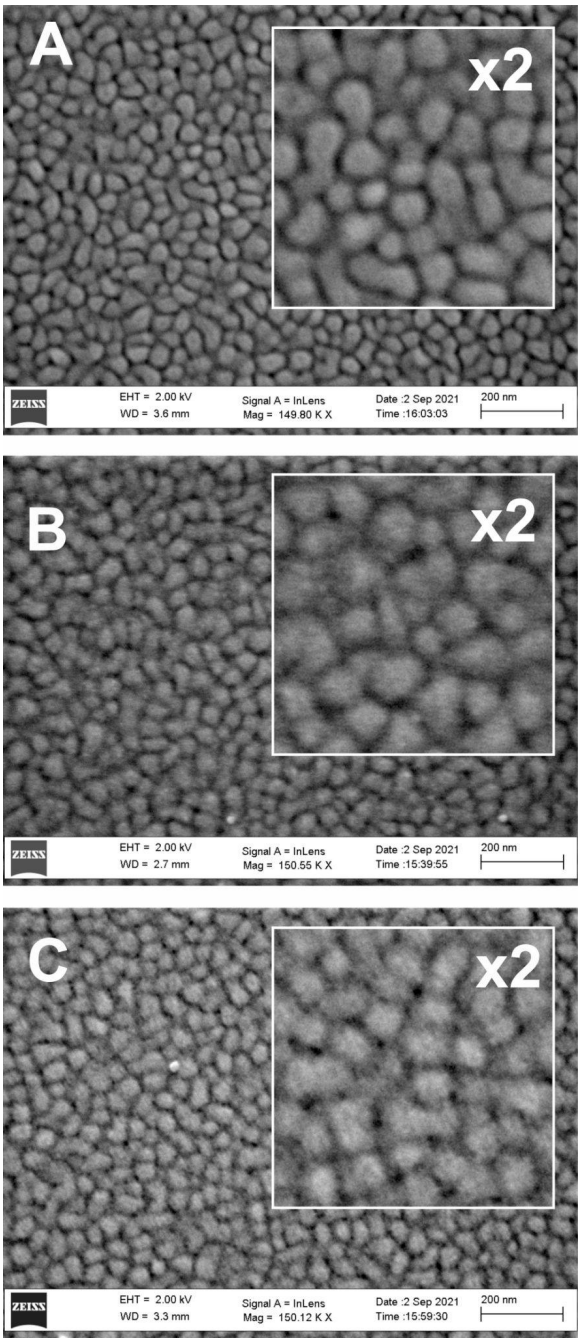

Fig. S3. SEM images of A) bare gold, B) PAPBA modified gold after previous functionalization with ATP, DTSSP and ncovS1 and C) ncovS1-MIP film modified gold surfaces.

S3. Optimization of ncovS1 sensor preparation

Selecting the optimal ncovS1-MIP film thickness in ncovS1 sensor

The performance of a MIP based sensor depends, to a great extent, on the film thickness. This is even of more importance when preparing MIP-based sensors for protein analysis. Thus, to optimize ncovS1-MIP film thickness for improved sensor performance, an increasing number of CV scans (5, 10, and 15 cycles) were explored during electrosynthesis of PAPBA. To evaluate the performance of the sensors, their responses to increasing ncovS1 concentrations (0.01-6.25 ng/ml) were analysed and the maximum response ($I_{n,max}$) determined by plotting adsorption isotherms that were fitted to the Langmuir model (Eq. S1):

$$I_n = (I_{n,max}C)/(K_D+C) \quad \text{(S1)}$$

where I_n and $I_{n,max}$ are the sensor responses at concentration C and at saturation respectively and K_D is the equilibrium dissociation constant. The Langmuir equation has proven useful and effective in understanding the adsorption mechanism of a target molecule with a MIP surface and is commonly reported in protein MIP research.

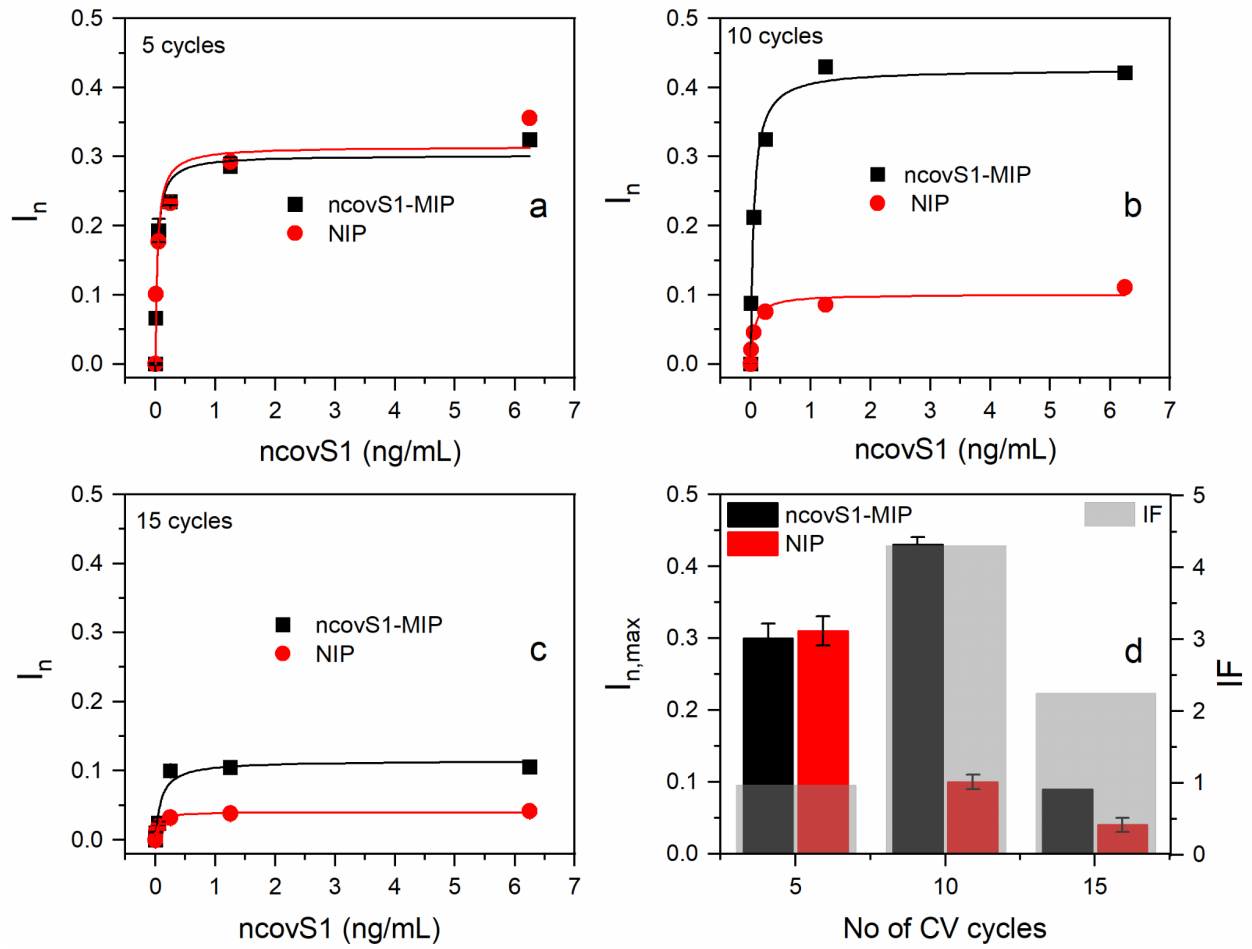

Fig. S4. (a-c) Adsorption isotherms and (d) maximum responses ($I_{n,max}$) of ncovS1-MIP and NIP prepared using different CV cycles (5, 10, 15) following 15 min incubation in increasing concentrations of ncovS1 (0.01; 0.05; 0.25; 1.25; 6.25 ng/ml) in PBS. *IF* values in (d) were calculated according to Eq. S1:

$$IF = I_{n,max}\ (ncovS1\text{-}MIP)/I_{n,max}\ (NIP) \quad \text{(S2)}$$

where $I_{n,max}$ *(ncovS1-MIP)* and $I_{n,max}$ *(NIP)* are the maximum responses obtained from ncovS1-MIP and NIP sensors respectively.

Similar experiments were performed on the NIP to appreciate the responses arising only from the specific interaction of ncovS1 on the tailor-made recognition sites. Fig. S4 shows that all ncovS1-MIP except that from 5 cycles, demonstrate higher binding responses than the NIP indicating the significance of imprinting ncovS1 in the polymer. The somewhat equal responses observed from ncovS1-MIP and NIP electrodeposited from 5 CV scan cycles can

be explained on the basis of the assumption that the polymer is too thin to allow for the creation of well defined ncov-S1 recognition sites.

Among the ncovS1-MIP and NIP prepared, 10 cycles shows the best performance as estimated by the *IF* value of 4.3 (Table S1). We can submit that at the thickness conferred by such CV cycles, the immobilized ncovS1 are well confined in the film thereby generating high affinity recognition sites at the surface of the film following template removal. Therefore, 10 CV scan was selected as the electrodeposition parameter to produce optimal ncovS1-MIP film on Au-TFME thus, is adopted for all subsequent experiments.

Table S1. $I_{n,max}$ obtained from ncovS1-MIP and NIP sensors electrodeposited from different numbers of CV cycles.

No of CV cycle	MIP	NIP	IF
5	0.30 ± 0.02	0.31 ± 0.02	1.0
10	0.43 ± 0.01	0.1 ± 0.01	4.3
15	0.1 ± 0.01	0.04 ± 0.01	2.5

Selecting the optimal time for incubating ncovS1 sensor in ncovS1 containing samples

The rebinding time of ncovS1 on ncovS1 sensor obtained from 10 CV cycle was optimized by incubating the sensor in PBS containing 0.05 ng/ml (K_D value) for different time intervals. As observed in Fig. S5, the responses increase sharply up to 15 min after which no further change is seen. This indicates that 15 min is the optimal rebinding time and was thus adopted subsequently.

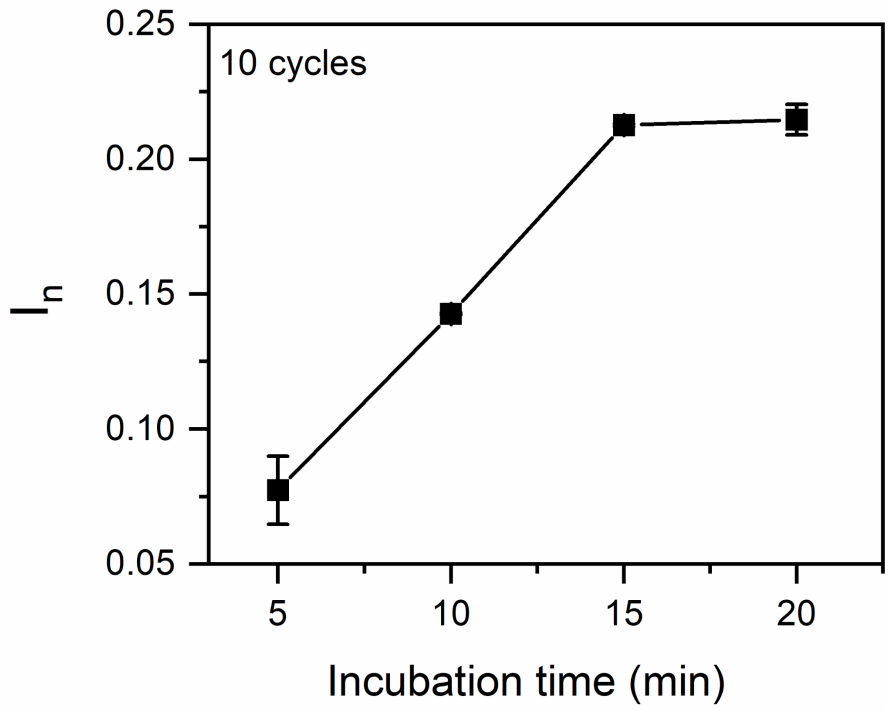

Fig. S5. Optimization of rebinding time of ncovS1 on ncovS1 sensor prepared from 10 CV cycles. The responses were obtained after incubation in PBS containing 0.05 ng/ml ncovS1.

S4. Structures of analytes used in the selectivity study

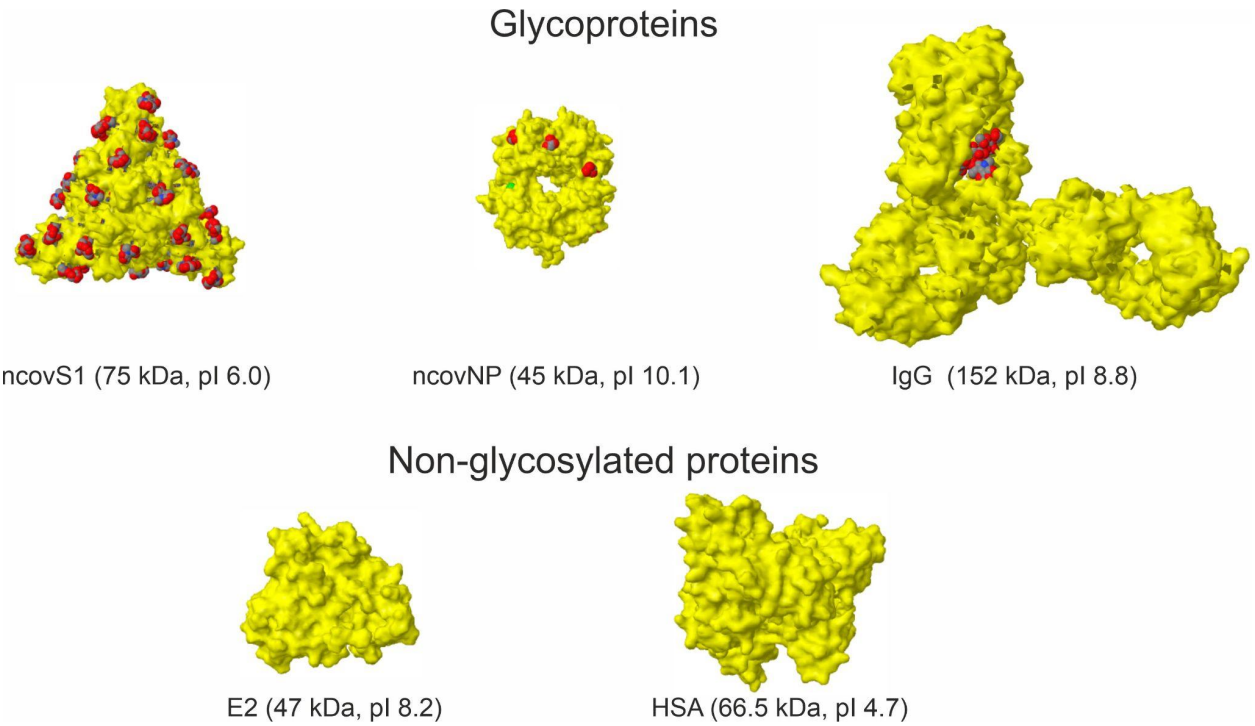

Fig. S6. 3D structure of ncovS1, ncovNP, IgG, HSA (monomeric form), and E2 proteins. The red spheres are oxygen atoms of carbohydrate residues in the glycoproteins.

S5. Study of ncovS1 sensor performance in sample preservation solution (SPS)

The clinical nasopharyngeal samples of COVID-19 patients were obtained from SYNLAB Eesti medical laboratory (Estonia) in sample preservation solution (SPS), (Jiangsu Mole Bioscience Co., Ltd). However, SPS contains Guanidine thiocyanate 20-30 w/w % which can interfere with sensor performance. Hence, to reduce the detrimental effects of this component in SPS, the samples were diluted in PBS.

To determine the exact dilution that would allow for accurate sensor performance, the sensor response following incubation in different diluted SPS solutions was studied. As observed in figure S6, 100 fold dilution i.e., 1:99 (SPS:PBS), does not suppress to a great extent, the sensor response yielding I_n value of 0.14 as compared to those of other dilutions (Table S2). Thus, ncovS1 solutions were prepared by spiking 100 fold diluted SPS solutions with the required amount of ncovS1 and the response increases linearly with ncovS1 concentration up to 250 fM (Fig. S7d).

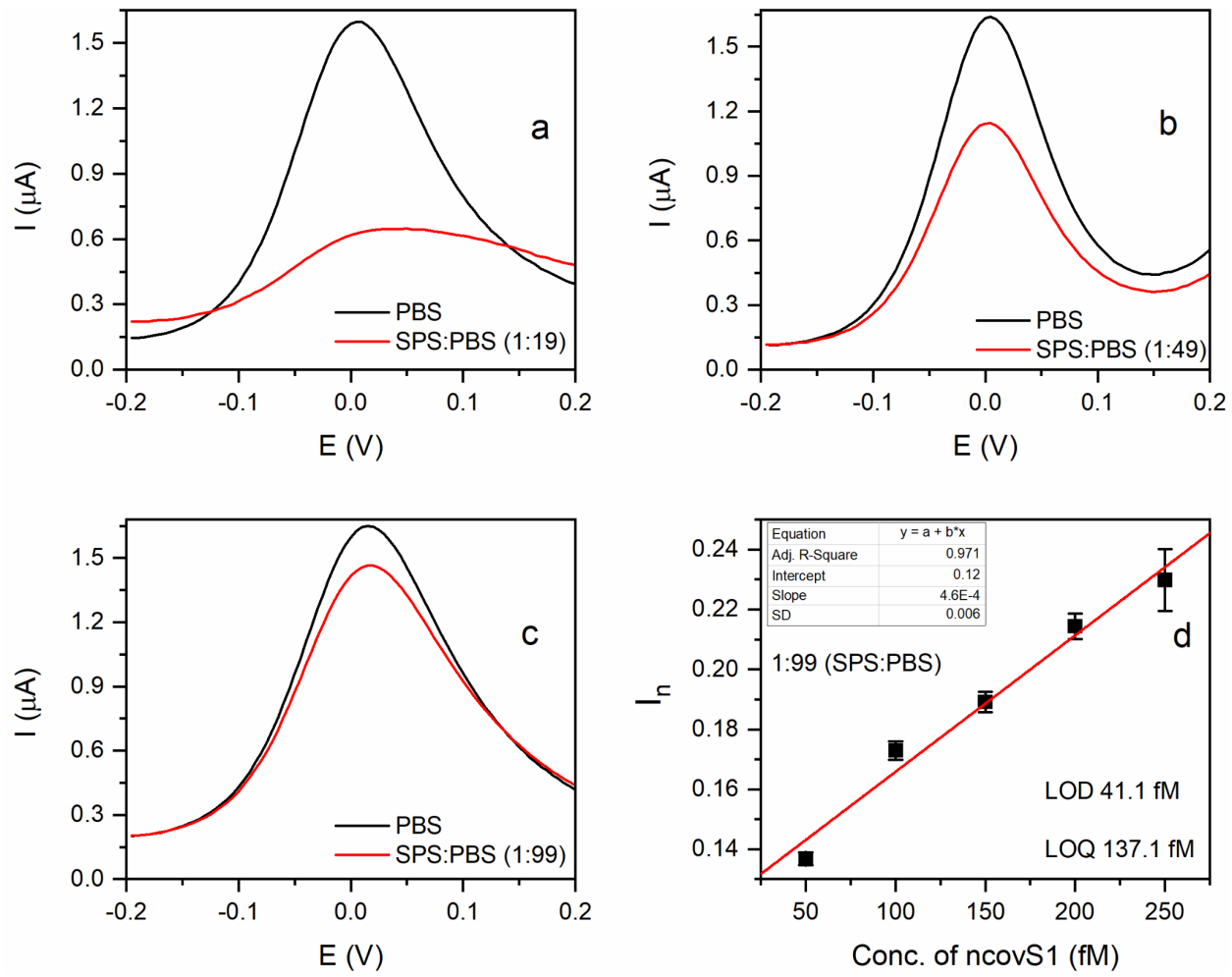

Fig. S7. (a-c) Square wave voltammograms (SWV) recorded in 1 M KCl solution containing a 4 mM redox probe $K_3[Fe(CN)_6]/K_4[Fe(CN)_6]$ on ncovS1 sensor following incubation in SPS diluted with different amount of PBS: (a) 1:19, (b) 1:49, (c) 1:99 (SPS:PBS). (d) Calibration plot of ncovS1 sensor obtained against increasing S1 concentration (50-250 fM) in 1:99 (SPS:PBS).

Table S2. ncovS1 sensor responses (I_n) upon incubation in different dilutions of SPS solutions.

Dilution (SPS:PBS)	$\boldsymbol{I_n}$
1:19	0.77
1:49	0.33
1:99	0.14

S6. Study of ncovS1 sensor performance in COVID-19 negative samples

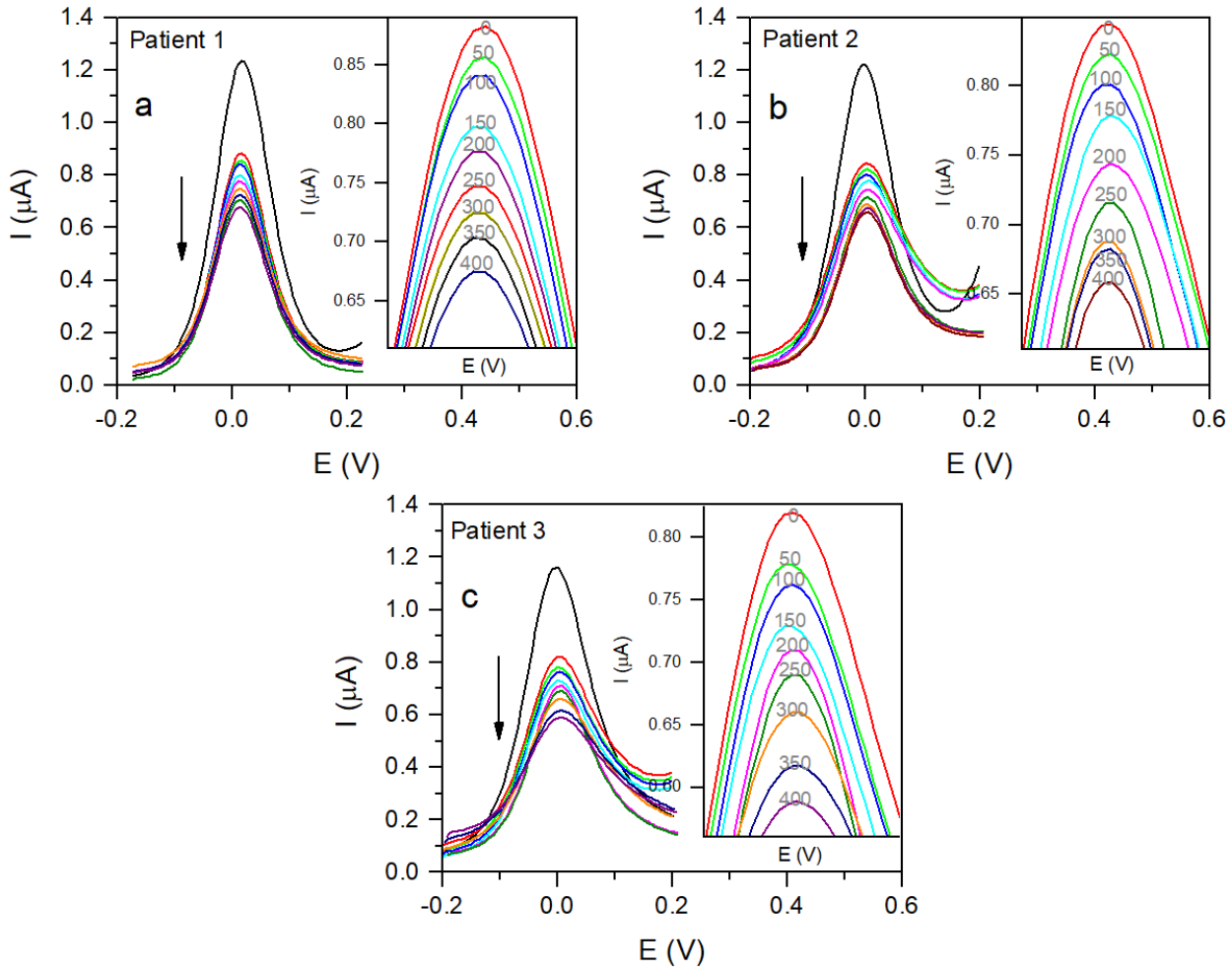

Fig. S8. (a-c) Square wave voltammograms (SWV) recorded in 1 M KCl solution containing a 4 mM redox probe $K_3[Fe(CN)_6]/K_4[Fe(CN)_6]$ on ncovS1 sensor following incubation in increasing concentrations of ncovS1 (0 to 400 fM). Numbers on the voltammograms of inset graphs represent ncovS1 concentrations in fM.

S7. Comparison of the performance of ncovS1 sensor with other sensor platforms for SARS-CoV-2 determination

Table S3. Electrochemical sensors for SARS-CoV-2 antigen detection.

Platform	Analyte	Receptor	LOD (pg/ml)	Analysis time[1] (min)	Ref
Graphene-based FET	S protein	SARS-CoV-2 spike antibody	0.001 (PBS); 0.1 (clinical sample[2])	Not found	[1]
MXene-graphene-FET	S protein	SARS-CoV-2 spike antibody	0.001 (PBS)	Not found	[2]
SPE/absorbing cotton padding/SWV	N protein and anti-N protein antibody complex; Competitive assay	N-protein	0.8 (PBS)	20	[3]
Graphene-functionalized SPE/(SWV)	S protein (S1 subunit)	SARS-CoV-2 spike antibody	Lowest detected conc. $2*10^7$	45	[4]
Magnetic beads-based SPE	S-protein N protein	SARS-CoV-2 spike antibody; SARS-CoV-2 nucleoprotein antibody	19000 (S); 8000 (N) (untreated saliva)	30	[5]
MIP-modified TFME	S-protein (S1 subunit)	ncovS1-MIP synthetic receptor	1.12 (PBS); 4.8 (clinical samples[3])	15	This work

[1]sensor incubation time with a sample solution before the electrochemical measurement.

[2]nasopharyngeal swabs suspended in universal transport medium (UTM) and inactivated by heating at 100 °C for 10 min.

[3]nasopharyngeal swabs suspended in sample preservation solution (SPS) diluted in PBS (1:99).

SPE - screen-printed electrode

SWV - Square Wave Voltammetry

S7. Point-of-care analysis

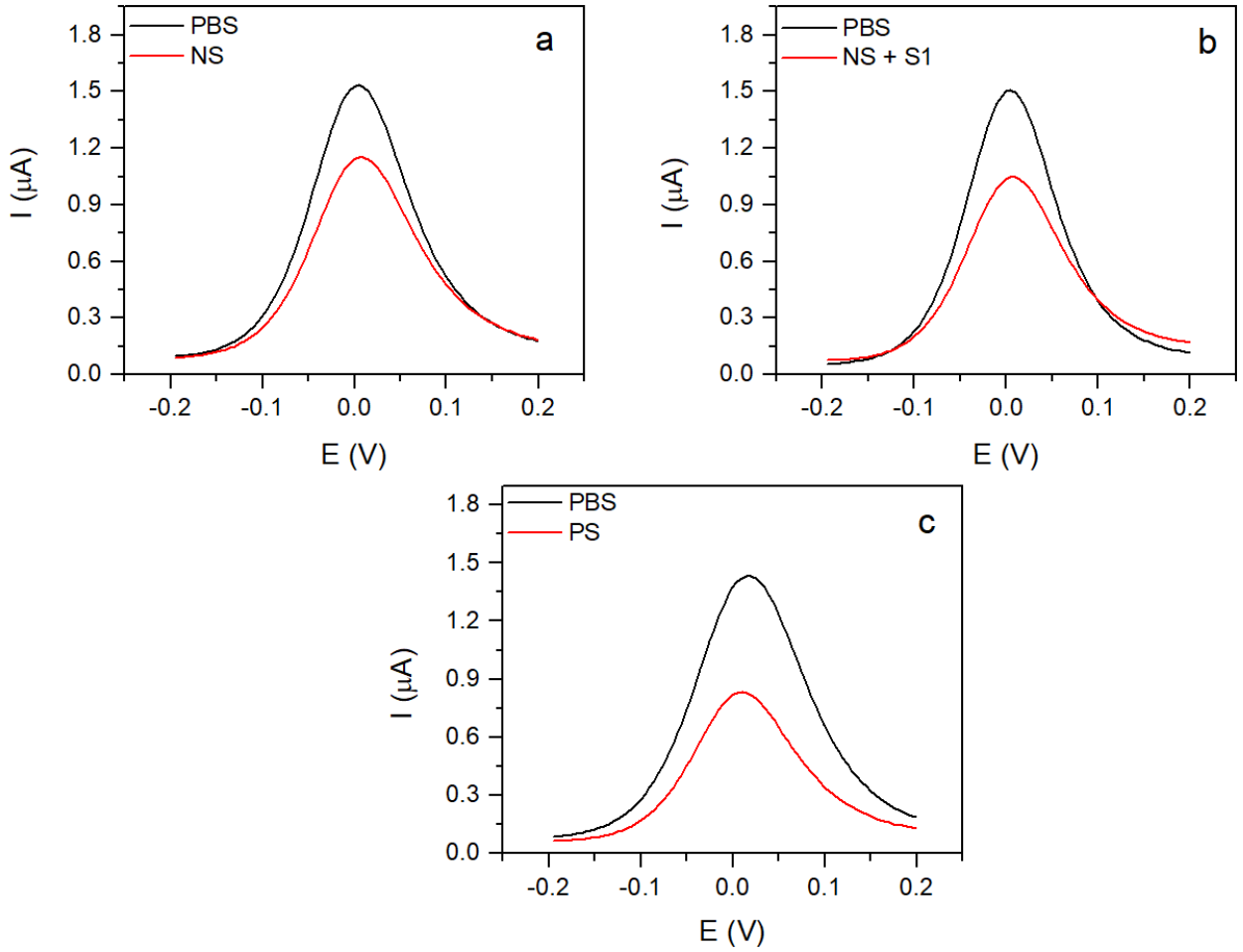

Fig. S9. Typical SWV voltammograms obtained from the sensor against (a) patient 1 COVID-19 negative sample (NS), (b) patient 1 NS spiked with 64 fM S1 (NS+S1) and (c) Patient 4 COVID-19 positive sample (PS). All measurements were performed using the ncovS1-MIP-modified chip connected to a portable potentiostat (EmStat3 Blue, PalmSens BV, The Netherlands).

References

[1] G. Seo, G. Lee, M.J. Kim, S.-H. Baek, M. Choi, K.B. Ku, C.-S. Lee, S. Jun, D. Park, H.G. Kim, Rapid detection of COVID-19 causative virus (SARS-CoV-2) in human nasopharyngeal swab specimens using field-effect transistor-based biosensor, ACS Nano. 14 (2020) 5135–5142. https://doi.org/10.1021/acsnano.0c06726.

[2] Y. Li, Z. Peng, N.J. Holl, Md.R. Hassan, J.M. Pappas, C. Wei, O.H. Izadi, Y. Wang, X. Dong, C. Wang, Y.-W. Huang, D. Kim, C. Wu, MXene–Graphene Field-Effect Transistor Sensing of Influenza Virus and SARS-CoV-2, ACS Omega. 6 (2021) 6643–6653. https://doi.org/10.1021/acsomega.0c05421.

[3] S. Eissa, M. Zourob, Development of a Low-Cost Cotton-Tipped Electrochemical Immunosensor for the Detection of SARS-CoV-2, Anal. Chem. 93 (2021) 1826–1833. https://doi.org/10.1021/acs.analchem.0c04719.

[4] B. Mojsoska, S. Larsen, D.A. Olsen, J.S. Madsen, I. Brandslund, F.A. Alatraktchi, Rapid SARS-CoV-2 Detection Using Electrochemical Immunosensor, Sensors. 21 (2021) 390. https://doi.org/10.3390/s21020390.

[5] L. Fabiani, M. Saroglia, G. Galatà, R. De Santis, S. Fillo, V. Luca, G. Faggioni, N. D'Amore, E. Regalbuto, P. Salvatori, G. Terova, D. Moscone, F. Lista, F. Arduini, Magnetic beads combined with carbon black-based screen-printed electrodes for COVID-19: A reliable and miniaturized electrochemical immunosensor for SARS-CoV-2 detection in saliva, Biosens. Bioelectron. 171 (2021) 112686. https://doi.org/10.1016/j.bios.2020.112686.